frontiers | Frontiers in Energy Research

TYPE Original Research
PUBLISHED 03 January 2025
DOI 10.3389/fenrg.2024.1509218

OPEN ACCESS

EDITED BY
Guobin Zhang,
Xi'an Jiaotong University, China

REVIEWED BY
Chuan Yi Foo,
Xiamen University, Malaysia
Dewei Wang,
North Minzu University, China

*CORRESPONDENCE
Leonardo Vivas,
leonardo.vivas@usm.cl

RECEIVED 10 October 2024
ACCEPTED 09 December 2024
PUBLISHED 03 January 2025

CITATION
Vivas L, Manquian C, Pacheco-Catalán DE, Márquez P and Singh DP (2025) Fast-track microwave-assisted synthesis of CdMoO4 and CdWO4 nanoparticles for hybrid rGO/NPs electrodes in high-performance supercapacitors.
Front. Energy Res. 12:1509218.
doi: 10.3389/fenrg.2024.1509218

Fast-track microwave-assisted synthesis of CdMoO4 and CdWO4 nanoparticles for hybrid rGO/NPs electrodes in high-performance supercapacitors

Leonardo Vivas[1]*, Carolina Manquian[2], Daniella Esperanza Pacheco-Catalán[3], Paulina Márquez[4] and Dinesh Pratap Singh[2]

[1]Department of Electrical Engineering, Universidad Técnica Federico Santa María, Santiago, Chile, [2]Physics Department, Millennium Institute for Research in Optics (MIRO), Faculty of Science, University of Santiago of Chile (USACH), Santiago, Chile, [3]Unidad de Energía Renovable, Centro de Investigación Científica de Yucatán, A. C. Carretera Sierra Papacal-Chuburná Puerto Km 5, Mérida, Mexico, [4]School of Engineering, Central University of Chile, Santiago, Chile

Fast and facile synthesis of nanomaterials is always a challenge for industrial applications in various sectors. In this work, $CdMoO_4$ and $CdWO_4$ nanoparticles are synthesized by using a fast and cost-effective microwave-assisted method. The synthesized nanoparticles are mixed with reduced graphene oxide (rGO), to form active electrode materials for supercapacitor and their electrochemical performances were studied in detail. The electrodes were prepared by simple mixtures of rGO/$CdMoO_4$ and rGO/$CdWO_4$, and electrochemical performance were measured in both, two- and three-electrode configurations. In general, both rGO/$CdMoO_4$ and rGO/$CdWO_4$ mixtures exhibit an increased specific capacitance (Cp) compared to pure rGO. Notably, the rGO/$CdMoO_4$ mixture shows a Cp exceeding 543 Fg^{-1} at a scan rate of 5 mVs^{-1}, which represents a significant improvement over rGO alone (Cp = 225 Fg^{-1}). This increase in Cp can be attributed to the higher surface area of the rGO/$CdMoO_4$ electrode material due to smaller size of $CdMoO_4$ nanoparticles and their intercalation between the rGO layers in comparison to the rGO/$CdWO_4$ electrode material. Furthermore, the rGO/$CdMoO_4$ mixture demonstrated 77% capacitance retention over 5,000 charge/discharge cycles in the two-electrode configuration. The promising electrochemical performance and rapid, low-cost synthesis suggest that these materials have great potential for further use in high efficiency energy-storage devices.

KEYWORDS

reduced graphene oxide, fast-track synthesis, CdMoO4, CdWO4, supercapacitors, hybrid architecture, bridging effect

1 Introduction

The growing population, lifestyle changes, and increased use of electrical devices have led to significant advancements in energy generation and storage technologies, prioritizing efficiency, safety, and cost-effectiveness (Liu et al., 2010). In this context, electroactive materials for energy storage devices such as supercapacitors have gained substantial attention owing to their high efficiency, long life cycles, and high-power density. However, although supercapacitors excel in power density, batteries and fuel cells generally offer higher energy densities (Dissanayake and Kularatna-Abeywardana, 2024; Long et al., 2015).

Carbon-based materials, particularly graphene and its derivatives, have been extensively studied as electrode materials for supercapacitors, specifically for electrical double-layer capacitors, due to their excellent physical and chemical properties, large surface area, low cost, and abundant electroactive sites (Sheoran et al., 2022; LI et al., 2017). Reduced graphene oxide (rGO) has shown promising results in electrochemical energy storage (Fu et al., 2011; Rajagopalan and Chung, 2014). To further enhance energy storage capacity, rGO has been mixed with various nanomaterials (Vivas and Singh, 2022; Kalia et al., 2024) and combined with transition metal oxides, showing great potential for supercapacitor applications (Cui and Meng, 2020; Shejini et al., 2024; Shelke et al., 2024; Raut and Sankapal, 2016; Cuéllar-Herrera et al., 2024).

Cd-based binary metal oxides, such as cadmium molybdate ($CdMoO_4$), are particularly promising as electrode materials. For example, Lui et al. demonstrated that $CdMoO_4$ nanorods exhibit excellent electrochemical properties as cathode materials in lithium-ion batteries, with a discharge capacity of 748 mAh g^{-1} (Liu and Tan, 2010). Additionally, Anitha et al. synthesized $PbMoO_4/CdMoO_4$ composites for supercapacitor electrodes, reporting a high Cp of 1840.32 Fg^{-1} at a current density of 1 Ag^{-1} (Anitha et al., 2019). In these studies, nanoparticles were synthesized by using the hydrothermal and chemical bath deposition methods.

Increasing the demand for low-cost and scalable processes, microwave-assisted synthesis has emerged as an attractive method for nanoparticle fabrication because of its simplicity, one-step nature, and scalability (Faraji and Ani, 2014). Microwave synthesis is not only a faster and more efficient method, but also a green chemistry method. It minimizes the energy required to generate the reaction, as well as reducing the use of solvents, making it an economical method (Zhu and Chen, 2014; Lehmann, 2007; Chan et al., 2021).

The versatility of the method and the short microwave exposure time needed to achieve nanoparticles, has generated a great deal of interest in making it scalable due to the low cost of the equipment required (Bermúdez et al., 2015; Ritter et al., 2024; Kim et al., 2016). The disadvantage of this method lies in the search for materials with a high degree of crystallinity, as it requires long calcination processes, but for nanostructured materials with low crystallinity, the process is ideal for applications that require characteristics such as high reactivity, larger specific surface areas and adsorption capacities, just to name few (Ritter et al., 2024).

In the case of supercapacitors this method is economical and efficient to make materials with high surface area. Due to it's advantages over other methods, we have used microwave-assisted synthesis to produce $CdMoO_4$ and cadmium tungstate ($CdWO_4$) nanoparticles, which has significantly reduced the synthesis time (Phuruangrat et al., 2011; Lim, 2012; Sofronov et al., 2012) of the nanoparticles. In this study, we demonstrate that active electrode based on rGO mixed with $CdMoO_4$ and $CdWO_4$ nanoparticles, in symmetric supercapacitor devices, enhance the specific capacitance compared to device with only rGO based electrodes. Graphene oxide (GO) was synthesized by a modified Hummers method, and rGO was obtained by using hydrazine as a reducing agent. $CdMoO_4$ and $CdWO_4$ nanoparticles were synthesized by using a fast and low-cost microwave radiation method. When comparing the specific capacitances (Cp), the $rGO/CdMoO_4$ and $rGO/CdWO_4$ composites exhibited significantly higher Cp values than rGO only. Specifically, the $rGO/CdMoO_4$ composite achieved a Cp greater than 673 F g^{-1} at a scan rate of 5 mV s^{-1}, compared to 265 F g^{-1} for pure rGO under the same conditions.

Previous studies have explored the photocatalytic applications of $rGO/CdMoO_4$ and $rGO/CdWO_4$ composites (Xu et al., 2015; Moghadam et al., 2019). However, the rapid synthesis of these materials and their electrochemical properties as supercapacitor electrode materials remain largely unknown and sparsely studied.

2 Experimental methods

All the chemicals used in the experiments were of analytical grade and utilized without any further purifications.

2.1 Synthesis of reduced graphene oxide

GO was synthesized by modified Hummer´s method (Marcano et al., 2010). First a beaker was kept at 5°C in an ice bath, and then 1 g of graphite and 100 mL of sulfuric acid were mixed, further with a dropwise addition of 6 g of potassium permanganate ($KMnO_4$) under constant stirring for 2 h. The solution was diluted by adding 400 mL of water under vigorous stirring for 1 h, resulting in the formation of GO. Furthermore, GO was reduced by using 20 mL of GO and 0.1 mL hydrazine was dissolved in 100 mL of distilled water under constant magnetic stirring for 30 min. The resulting solution was washed several times with deionized water and dried in a freeze dryer.

2.2 Fast-track synthesis of nanoparticles of $CdMoO_4$ y $CdWO_4$

For the synthesis of $CdMoO_4$ nanoparticles first 3.84 g of $Cd(SO_4)\cdot H_2O$ was dissolved in 25 mL of ethylene glycol, under constant magnetic stirring. Separately, 1.21 g of $Na_2MoO_4\cdot 2H_2O$ powder was dissolved in 25 mL of ethylene glycol solution (approx. 20 min). Both solutions were mixed and heated at 140 °C for 6 min in a microwave with controlled temperature.

The same procedure was repeated for the synthesis of $CdWO_4$ nanoparticles by using $Na_2WO_4\cdot 2H_2O$ instead of $Na_2MoO_4\cdot 2H_2O$ only.

TABLE 1 Proportion of mass used in each mixture and active mass for the two- and three-electrode configurations.

Sample	Proportion of mass used in each mixture (%)		Active mass used in each configuration (mg)	
	rGO	NPs	Two-electrode	Three-electrode
rGO	100	—	18.20	54.41
rGO/$CdMoO_4$	70	30	13.61	50.38
rGO/$CdWO_4$	70	30	15.26	53.90

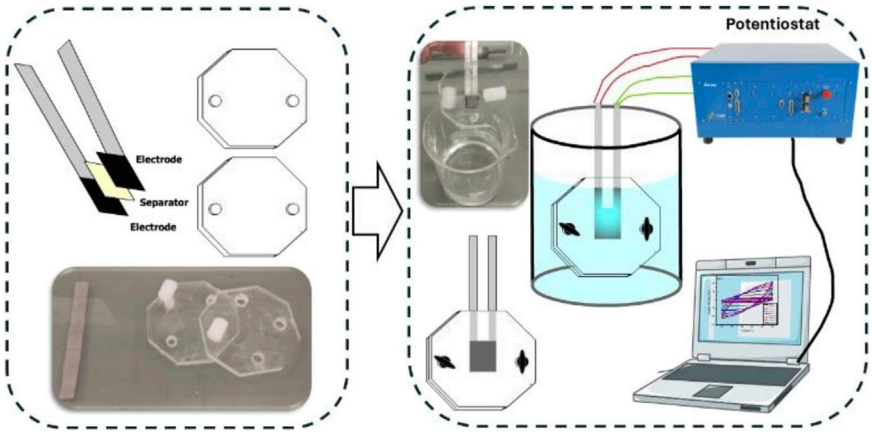

FIGURE 1
Assembly of the two-electrode configuration.

2.3 Fabrication of rGO/$CdMoO_4$ and rGO/$CdWO_4$ based electrodes for supercapacitors measurements

2.3.1 Electrode preparation

The electrodes were fabricated by using an active material, consisting of 70% of rGO by mass and 30% of $CdMoO_4$ or $CdWO_4$ by mass resulting in to rGO/$CdMoO_4$ and rGO/$CdWO_4$ composites. These ratios were selected based on our previous studies, in which a mixture of 70% rGO and 30% NPs demonstrated superior electrochemical performance. Table 1 details the mass of each component used in the mixtures (Vivas et al., 2022)

The composites were prepared by mixing rGO and NPs in ethanol followed by ultrasonication for 2 h. To prepare the electrode paste, an ethanol/rGO/NP mixture was combined with polytetrafluoroethylene (PTFE) binder (Sigma-Aldrich, St. Louis, MO, United States), and conductive carbon black (Super P conductive; Alfa Aesar, UK). The final paste consisted of 20 wt% carbon black, 10 wt% PTFE, and 70 wt% active material (Table 1). This mixture was stirred for 10 min and sonicated for 20 min until a viscous consistency was obtained.

2.3.2 Characterization of the materials

The surface morphology and microstructures of the resulting samples were characterized by Scanning electron microscopy (SEM, Zeiss at 30 kV), and the crystalline nature and structure were characterized by powder X-ray diffraction (pXRD) analysis done by Shimadzu XRD 6000 diffractometer with a Cu Kα radiation source and operated by XRD-6000 software, in the range of 2θ: 10°–65°. Raman spectroscopy, provided by NRS-4500 Jasco, is equipped with a 532 nm laser.

2.3.3 Electrochemical measurements

To make a comparative study between the active electrode materials and rGO, an electrochemical study was performed separately for each composite and rGO too.

The electrochemical performance of the samples rGO, rGO/$CdMoO_4$, and rGO/$CdWO_4$ were measured by a potentiostat/galvanostat BioLogic Science Instrument equipped with an impedance module. All data analyses were performed by using EC-Lab V11.34 software.

First, an assembled three-electrode system was used to obtain optimum material performance in a 6 M KOH electrolyte solution. A graphite rod was used as counter electrode (CE), an Ag/AgCl electrode as a reference electrode (RE), and the active material electrode was utilized as a working electrode (WE). Cyclic voltammetry (CV) was performed at different sweep rates between 5 and 250 mVs^{-1} and over a potential window of −1 to 0 V. Electrochemical impedance spectroscopy (EIS) was performed with a sinusoidal amplitude of 10 mV against the OCP over a frequency range of 0.02 Hz–100 kHz.

Finally, a symmetrical supercapacitor (SSC) was assembled with a two-electrode configuration by placing two opposing working

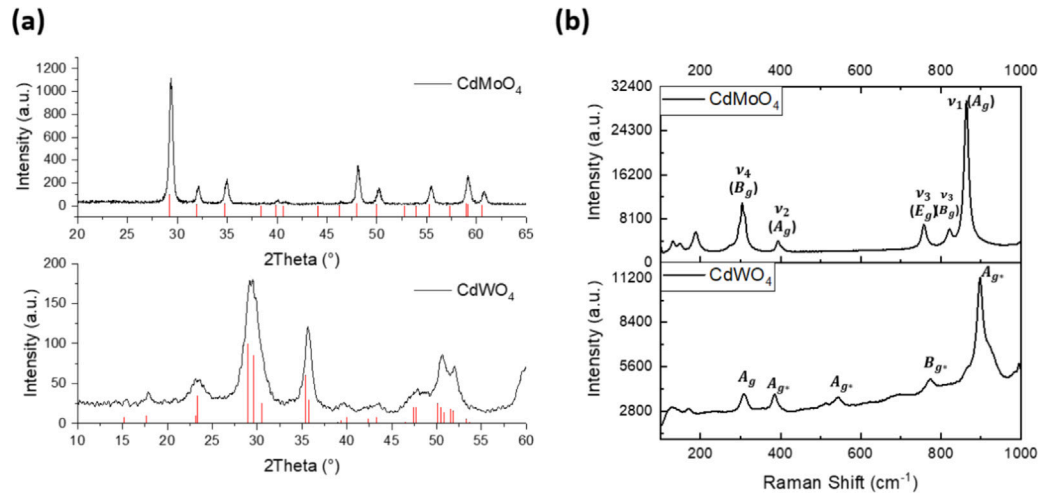

FIGURE 2
(A) XRD analysis and **(B)** Raman spectroscopy of the $CdMoO_4$ and $CdWO_4$ nanoparticles synthesized by microwave assisted method.

electrodes and filter paper between them to avoid short circuits. The assembly was immersed in a 6M KOH solution, as shown in Figure 1. Cyclic voltammetry (CV), electrochemical impedance spectroscopy (EIS), and charge/discharge (CD) studies were performed using the same parameters as those used for the three-electrode configuration.

The specific capacitance of the three-electrodes and two-electrodes configurations was calculated from cyclic voltammetry curves at different scan rates by fllowing Equations 1, 2.

$$C_s = \frac{\int Idv}{\Delta V\, v\, m}\left(\mathrm{Fg}^{-1}\right), \text{Three} - \text{electrode configuration} \quad (1)$$

$$C_s = \frac{\int Idv}{2\Delta V\, v\, m}\left(\mathrm{Fg}^{-1}\right), \text{Two} - \text{electrode configuration} \quad (2)$$

where C_S is the specific capacitance (Fg^{-1}), I is the current (A), ΔV is the potential window (V), υ is the scan rate (mVs^{-1}), and m is the active material mass (g).

The Energy Density and Power Density were calculated as follows:

$$E_D = \frac{1}{2}C_s\left(\Delta V\right)^2\ \left(\mathrm{Wh\,kg}^{-1}\right), \quad (3)$$

$$P_D = E_D/\Delta t\ \left(\mathrm{W\,kg}^{-1}\right), \quad (4)$$

where Δt is the cell-discharge rate.

3 Results

3.1 Structural characterization

Figure 2A shows the XRD patterns of the $CdMoO_4$ and $CdWO_4$. For the sample $CdMoO_4$, the characteristic diffraction peaks corresponding to a tetragonal phase of $CdMoO_4$ are consistent with the reported data (JCPS, card No. 01-088-0,182), where the lattice constants are a = 5.156 Å and c = 11.196 Å. For the sample $CdWO_4$, the diffraction peaks correspond to the monoclinic phase of $CdWO_4$, corresponding to base data JCPS, card No. 00-013-0,514. In both cases, the efficacy of microwave synthesis was demonstrated, and the nanoparticles showed a well-defined crystalline phase.

Figure 2B shows that the Raman spectrum of $CdMoO_4$ has a peak at 863.3 cm^{-1}, which is assigned to the ν_1 (A_g) symmetric stretching vibration mode of the [MoO_4] cluster in the $CdMoO_4$ structure. The peaks at 821.3 and 757 cm^{-1} were assigned to the significant antisymmetric stretching ν_3 (B_g) and ν_3 (E_g) vibration modes of the $CdMoO_4$ structure, respectively. Furthermore, the peaks at 393 and 304 cm^{-1} were assigned to the weaker ν_4 (B_g), and stronger ν_2 (A_g) modes of the [MoO_4] tetrahedrons (Kadam et al., 2018), whereas the peaks at 188 and 148 cm^{-1} were assigned to medium and very weak modes of R, and the peak at 131 cm^{-1} was assigned as T vibration mode (Jayaraman et al., 1995). The Raman spectra of $CdWO_4$ showed an intense peak of vibration modes located at 898 cm^{-1}, corresponding to the normal W-O vibrations. The peak modes located at 775 cm^{-1} correspond to WO_2, while the peak at 697 cm^{-1} corresponds to the asymmetric stretching modes of the W-O-W bridges. The vibration modes located at 514 and 543 cm^{-1} can be assigned to the modes arising from the symmetric W-O-W stretching modes. The peak at 308 cm^{-1} can be assigned to the symmetric stretching of CdO_6 octahedra, whereas bands below 300 cm^{-1} can be assigned to out-of-plane W-O deformations (Daturi et al., 1997).

The panel Figure 3 represents the SEM images of the rGO, $CdMoO_4$ and $CdWO_4$ nanoparticles. Figure a–c are the low and high magnification images of synthesized rGO sample. Figure (d–f) represents the SEM images of the $CdMoO_4$ nanoparticles which shows very homogeneous smaller size particles than observed in case of $CdWO_4$ Figure (g–i). The $CdMoO_4$ nanoparticles showed porous structures, similar to those reported by Phuruangrat et al. (2011), homogeneous, with regular sizes and shapes, whereas the morphology of the $CdWO_4$ nanoparticles was homogeneous but irregular shape, as reported by Kumar et al. (2024) by using hydrothermal method. By using the ImageJ software, the average particle size was calculated as represented by the histograms, depicted in the inset of the Figure (d) and (g). The analysis

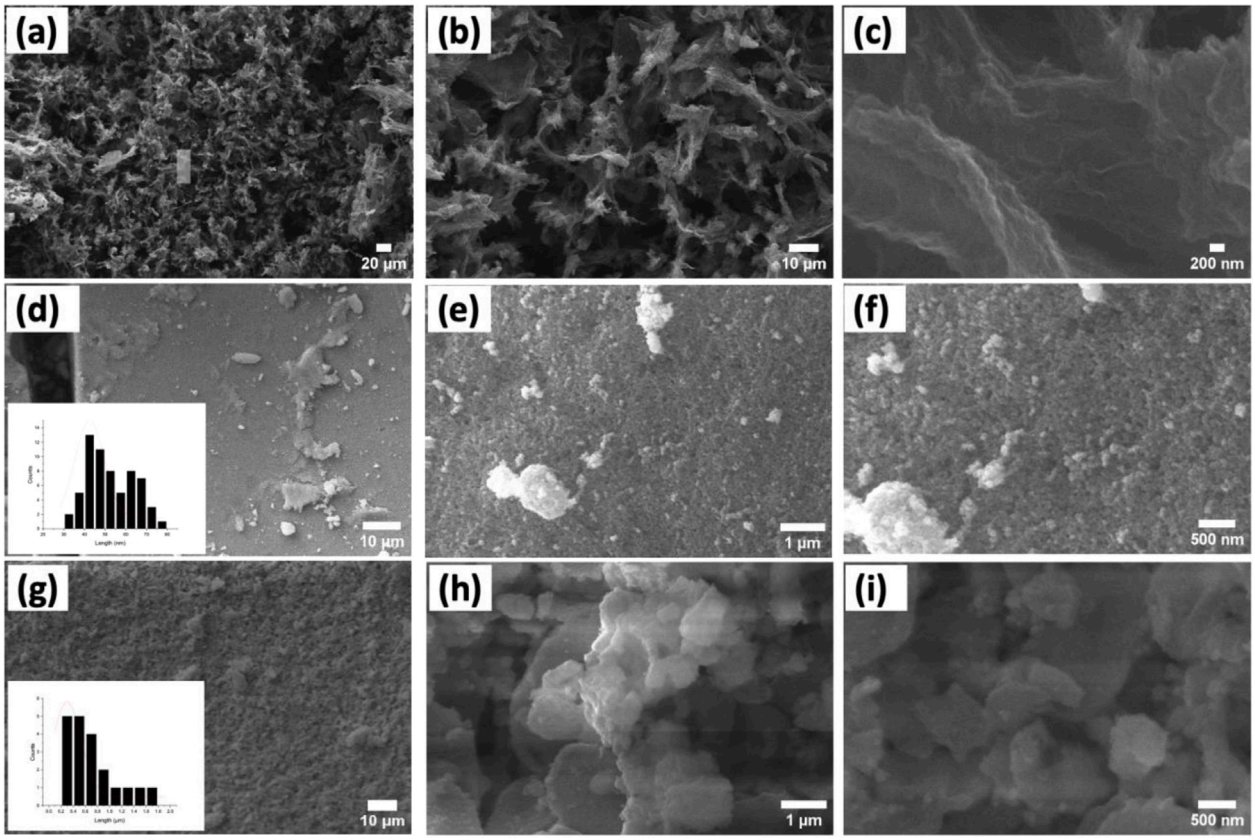

FIGURE 3
Low and high magnifications SEM images of rGO **(A–C)**, $CdMoO_4$ nanoparticles **(D–F)** and $CdWO_4$ nanoparticles **(G–I)**.

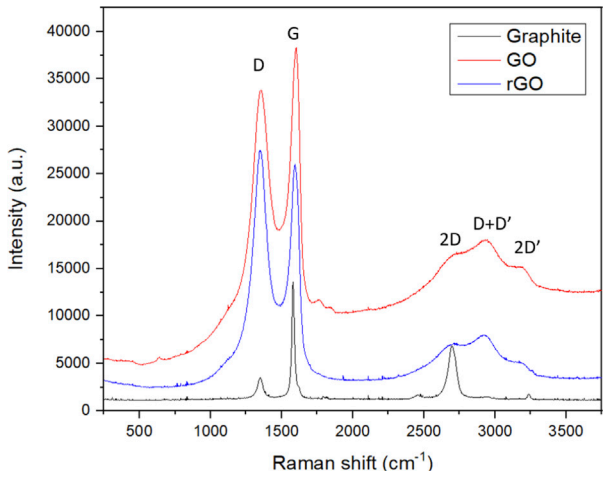

FIGURE 4
Comparative Raman spectroscopy of graphite, GO, and rGO.

showed that the average particles size of the $CdMoO_4$ and $CdWO_4$ nanoparticles are ~ 42.5 nm and ~ 300 nm respectively.

The Raman spectrum of the graphite, GO, and synthesized rGO, is shown in Figure 4, where the incorporation of hydrazine to GO, an effective reduced rGO was obtained (Ren et al., 2011; Wang et al., 2013; Das et al., 2024).

The spectrogram shows that for the rGO sample, the main peak of graphene corresponding to G band, located at ~1,593 cm^{-1}, is associated with the doubly degenerate phonon mode at the Brillouin zone center, corresponding to the allowed E2 g mode arises from sp^2 hybridized C-C bond stretching. The second characteristic peak corresponds to the 2D band peak and is located at ~2,706 cm^{-1}, represent a two-phonon lattice vibrational process (Ferrari, 2007). In addition, for rGO, it was observed that the increase of band D, as the disorder band or the defect band, representing a ring breathing mode from the sp^2 carbon ring, and the band D + D′, located at ~1,351 cm^{-1} and ~2,923 cm^{-1}, respectively, and these peaks were observed due to defects in the rGO structure. The graphitization degree of the carbon material was characterized by the relationship between the ID/IG ratio, corresponding to the intensities of bands D and G. For rGO, the relationship was ID/IG = 1.06. This suggests that the synthesized rGO had a high defect density, which could be linked to chemical interactions, surface dislocations, corrugation, or vacancies. Furthermore, the presence of the two-dimensional (2D) peak at 2,697 cm^{-1} and the D + D′ peak at 2,933 cm^{-1} indicates improved graphitization and the existence of few-layered graphene sheets. The 2D′ peak at 3,184.6 cm^{-1} corresponds to the overtone of the D′ peak. Because the 2D and 2D′ peaks arise from a process in which momentum conservation is satisfied by two phonons with opposite wavevectors, no defects are required for their activation, and they are therefore always present (Vivas et al., 2022; Alam et al., 2017).

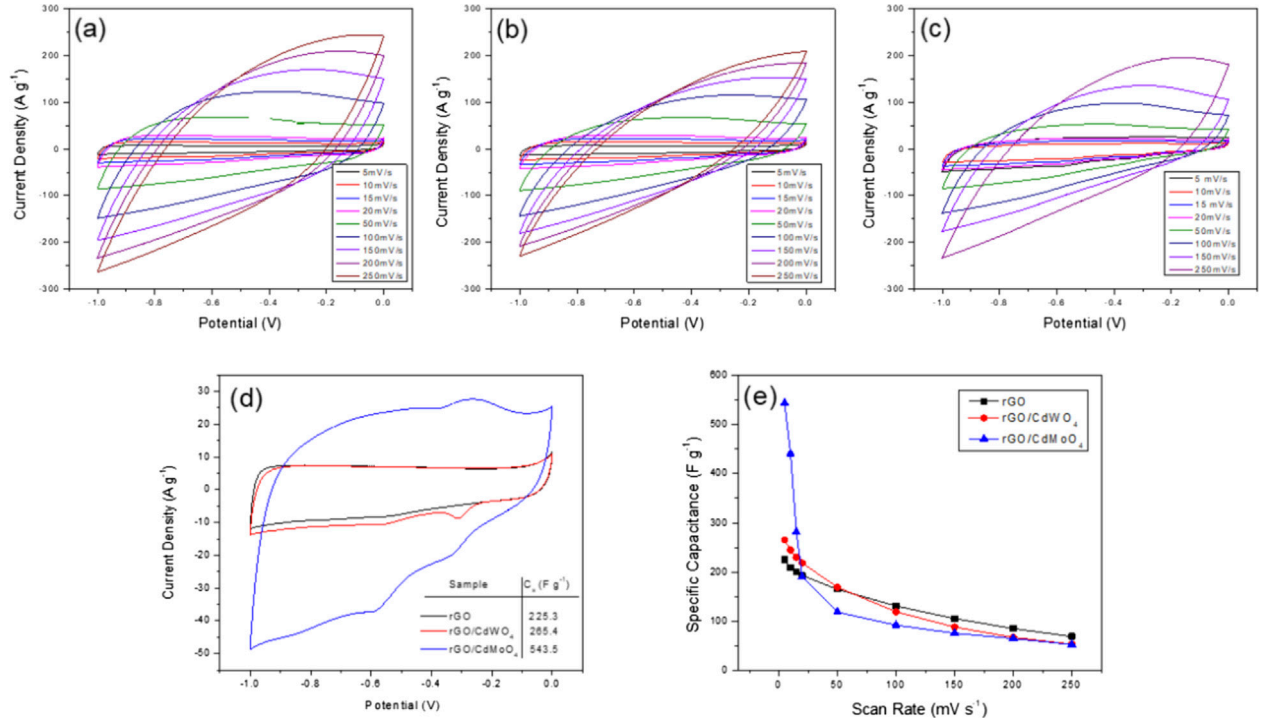

FIGURE 5
Cyclic voltammetry performance of **(A)** rGO, **(B)** rGO/$CdWO_4$, and **(C)** rGO/$CdMoO_4$ at different scan rates. **(D)** Show the CV curves of the electrodes for a constant scan rate of 5 mVs^{-1}. **(E)** Specific capacitance at different scan rates for three-electrode configuration.

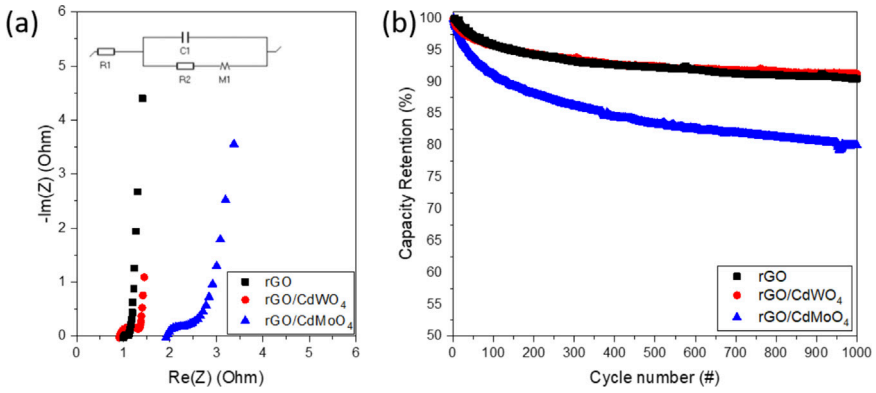

FIGURE 6
(A) Nyquist plot and **(B)** cyclability up to 1,000 cycles for rGO, rGO/$CdWO_4$, and rGO/$CdMoO_4$ samples.

3.2 Electrochemical characterization

3.2.1 Three-electrodes configuration

Figure 5 shows the Cyclic Voltammetry (CV) curves of (a) rGO, (b) rGO/$CdWO_4$, and (c) rGO/$CdMoO_4$ electrodes in 6 M KOH solution in a potential window of −1 to 0 V, for sweep rates of 5, 10, 15, 20, 50, 100, 150, 200, 250 mVs^{-1}. As shown in the figure, the CV profiles correspond to electric double-layer capacitor behaviour (EDLCs), a typical characteristic of carbon-based materials (Dubey and Guruviah, 2019; Wang et al., 2021).

Figure 5D shows the cyclic voltammetry (CV) for each electrode at a scan rate of 5 mVs^{-1}. The specific capacitance of each electrode was calculated by using Equation 1, and the results are presented in the inset of the graph. It is evident that the CV area of the rGO/$CdMoO_4$ electrode is significantly larger than those of the other two electrodes. Moreover, when comparing the specific capacitances, the rGO/$CdMoO_4$ electrode showed a value higher than double that of the others. This demonstrates that the presence of $CdMoO_4$ nanoparticles in rGO increases both the surface area and the ion polarization within the electrolyte.

TABLE 2 Value of the equivalent circuit corresponding to the Nyquist plots of the samples.

Sample	R1 (Ω)	C1 (mF)	R2 (Ω)	M1 (Ω)
rGO	1.11	0.32	0.14	13.34
rGO/$CdWO_4$	0.91	0.50	0.59	11.01
rGO/$CdMoO_4$	2.25	0.67	0.12	2.80

Figure 5E shows the calculated specific capacitance of the rGO, rGO/$CdWO_4$, and rGO/$CdMoO_4$ samples as a function of the scan rate by using Equation 1. The specific capacitance decreased from 255 to 69 Fg^{-1} for rGO, 265 to 54 Fg^{-1} for rGO/$CdWO_4$, and 673 to 53 Fg^{-1} for rGO/$CdMoO_4$, for a scan rate of 5–250 mVs^{-1}, showing that rGO doped with $CdWO_4$ and $CdMoO_4$ nanoparticles increased the specific capacitance of rGO. The decay of the specific capacitance is observed as a function of the scan rate, where for fast scan rates, the specific capacitance per unit of mass is given because of the porosity in the electrode surface, with the ions not having the possibility of entering the pore, an effect that occurs at low scanning rates, where the ions have enough time to access the pores and more interior active sites of the electrode material (Shabani Shayeh et al., 2015).

Electrochemical impedance spectroscopy (EIS) was performed for the rGO, rGO/$CdWO_4$, and rGO/$CdMoO_4$ electrodes to generate Nyquist plots, as shown in Figure 6A, in the frequency of 0.02 Hz–100 kHz. The Nyquist diagram shows a semicircle at high frequencies followed by a sloping line in the low-frequency region. To analyse the Nyquist plots, we utilized the equivalent circuit for model fitting of the Nyquist curves observed in the image, where Table 2 shows the values for the equivalent circuit.

Figure 6B shows the capacity retention of the samples for 1,000 cycles of charge and discharge, with capacity retentions of 80.0, 91.3, and 90.5% for the rGO/$CdMoO_4$, rGO/$CdWO_4$, and rGO samples, respectively, at a current density of 1 Ag^{-1}.

3.2.2 Two-electrode configuration

The electrochemical properties of the composites were evaluated and compared at the device level by using an arrangement of two electrodes for supercapacitor applications. The performance of the supercapacitor as a device forming a symmetric supercapacitor was measured by using cyclic voltammetry (CV), electrochemical impedance spectroscopy (EIS), and galvanostatic charge/discharge (CD).

Figure 7 shows the performance of CV curves for the samples (a) rGO, (b) rGO/$CdWO_4$, and Figure (c) rGO/$CdMoO_4$ for 6M KOH electrolyte solution, in a potential window of −1 to 0 V, which show close curve corresponding to ideal capacitive behaviour. This effect is visible more clearly in Figure (d), which shows the CV curves performed at a constant scan rate of 5 mV^{-1}. The calculated specific capacitances with Equation 2 obtained for a 5 mVs^{-1} are 20.3, 38.2, and 99.1 Fg^{-1} for rGO, rGO/$CdWO_4$, and rGO/$CdMoO_4$, respectively. Figure 7E shows the specific capacitance as a function of scan rate, where we obtained a specific capacitance of 20 to 4 Fg^{-1} for rGO, 38 to 12 Fg^{-1} for the composite rGO/$CdWO_4$, and 99 to 21 Fg^{-1} for the composite rGO/$CdMoO_4$, at a scan rate of 5–250 mVs^{-1}, respectively. It

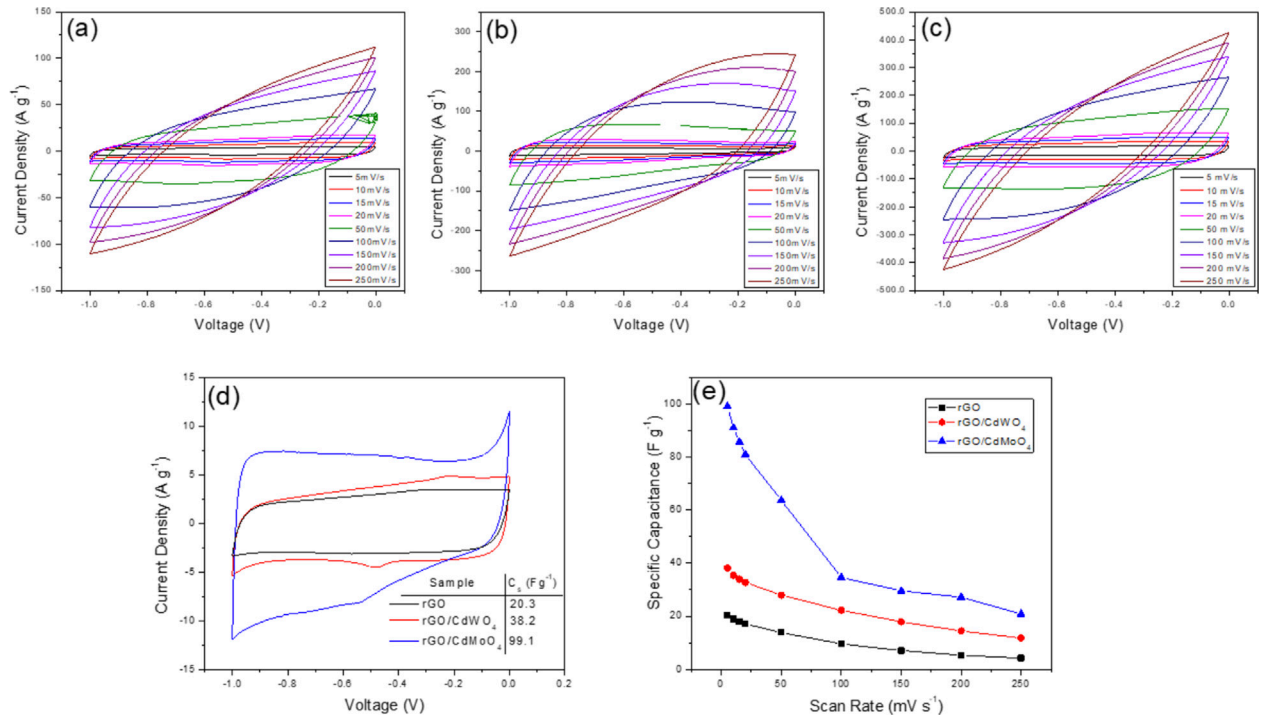

FIGURE 7
Cyclic voltammetry performance of **(A)** rGO, **(B)** rGO/$CdWO_4$, and **(C)** rGO/$CdMoO_4$ at different scan rates. **(D)** Show the CV curves of the electrodes for a constant scan rate of 5 mVs^{-1}. **(E)** Shows the specific capacitance at different scan rates for two-electrode configuration.

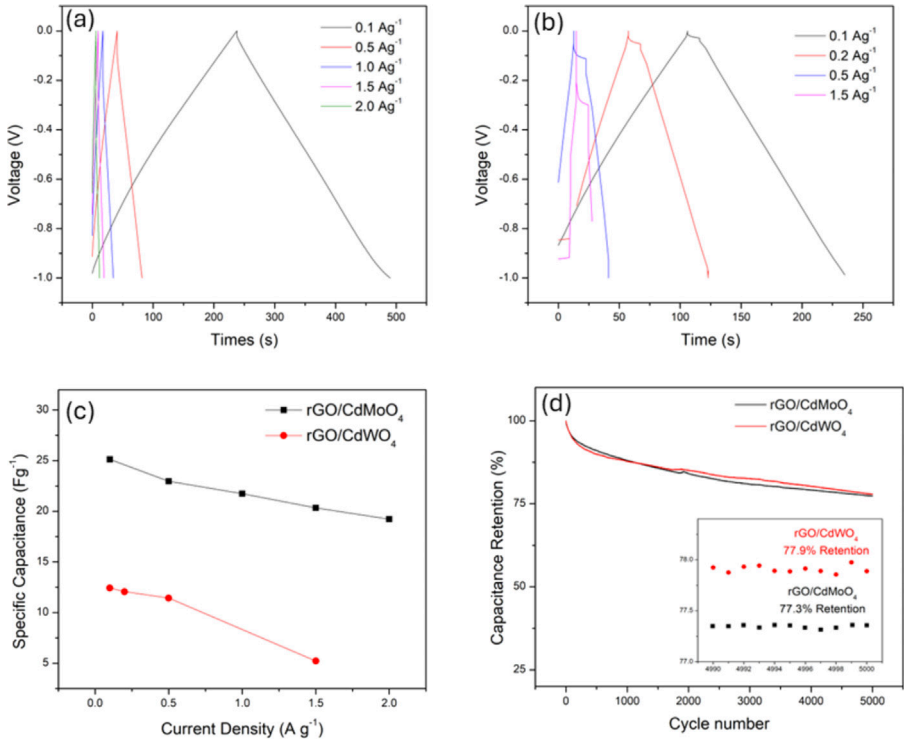

FIGURE 8
Charge–discharge curves for different current densities of $rGO/CdMoO_4$ **(A)** and $rGO/CdWO_4$ **(B)**. Specific capacitance **(C)** and capacitance retention of the composites after 500 cycles **(D)**.

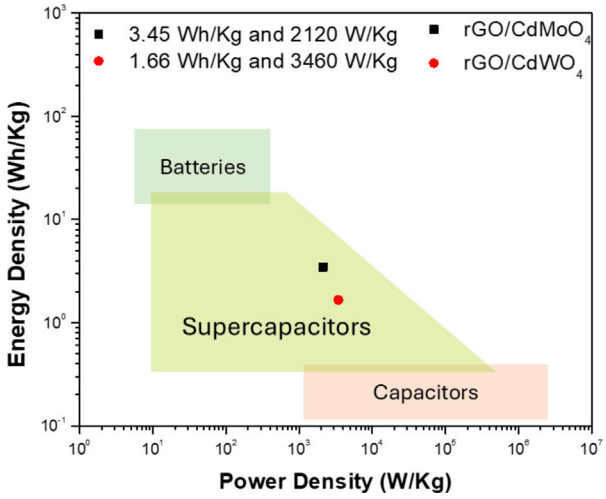

FIGURE 9
Ragone plots for the two-electrode configuration of $rGO/CdMoO_4$ and $rGO/CdWO_4$ electrodes.

represents that that the incorporation of nanoparticles of $CdWO_4$ and $CdMoO_4$, increase the performance not only of the three-electrode configuration but also for a cell devices, and superior performance was observed for the composite $rGO/CdMoO_4$.

Figure 8 shows the charge and discharge curves for different current densities, and it is observed that for the $rGO/CdMoO_4$, the performance corresponds to double layer electrode. The calculated specific capacitance, decreased from 25.1 to 19.2 Fg^{-1} for $rGO/CdMoO_4$ electrode, and from 12.4 to 5.2 Fg^{-1} for $rGO/CdWO_4$, electrode by using a current density of 0.1–2.0 Ag^{-1}, respectively. Figure 8D shows the capacitance retention of the composites for 5,000 cycles at 1 Ag^{-1}, where it is observed that the capacitance retention was 77.9% and 77.3% for $rGO/CdWO_4$ and $rGO/CdMoO_4$, respectively.

To compare the performance of the proposed devices, considering all energy storage devices, we present a Ragone plot of the energy density and power density, as shown in Figure 9, calculated by using Equations 3, 4. It is clear that the devices fabricated with rGO/NPs presented in this work exhibit the typical characteristics of a supercapacitor, with high power and energy densities that are comparable to those of other devices.

In our case, the two-electrode configuration of $rGO/CdMoO_4$ shows a higher energy density than $rGO/CdWO_4$, which is consistent with the fact that the specific capacitance is greater when analyzing cyclic voltammetry measurements. This implies a higher energy storage capacity. The energy and power density values of our devices are comparable to those of other energy storage devices, demonstrating the feasibility of using $CdMoO_4$ and $CdWO_4$ nanoparticles mixed with rGO in the fabrication of energy storage devices. This system proves to be a very promising candidate for future studies as a supercapacitor, particularly given its low cost and the simplicity and speed of the nanomaterials synthesis.

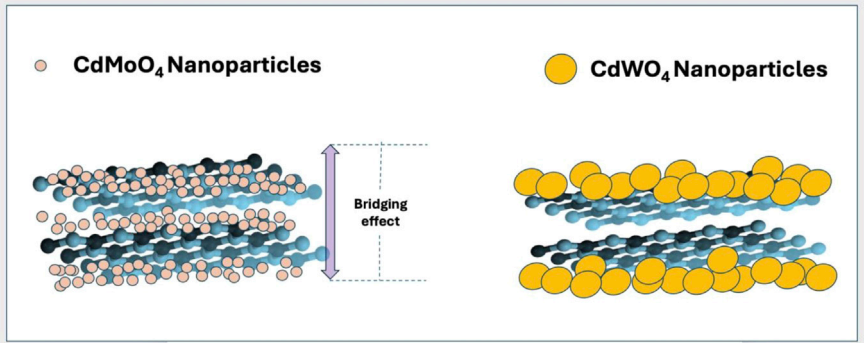

FIGURE 10
Tentative explanation of the bridging effect and better performance of supercapacitor based on rGO/$CdMoO_4$ material.

TABLE 3 comparison of results for the two-electrode configuration.

Sample	Electrolyte	Specific capacitance [F/g]	% retention (cycles)	Ref.
$CuMnO_2$-rGO/NF	2M KOH	93 at 2 Ag^{-1}	96, 7 (4,000)	Bahmani et al. (2019)
rGO/MnO_2	1M Na_2SO_4	144 at 1 mA	98, 7 (5,000)	Vimuna et al. (2022)
$NiCo_2S_4$/rGO	6M KOH	131.5 at 7,5 $mAcm^{-2}$	87, 8 (5,000)	Zhao (2024)
$Cd(OH)_2$	1M NaOH	267 at 5 mVs^{-1}	86 (1,000)	Patil et al. (2015)
CdO/NF	6M KOH	109 at 2 $mAcm^{-2}$	130 (5,000)	Chang et al. (2007)
CF-NSs-KN/I_2	2M $ZnSO_4$	291.5 $mAhg^{-1}$ at 0.5 Ag^{-1}	97.2 (20,000)	Sun et al. (2023)
A-MnO_x //HPC	1M $Ca(NO_3)_2$	175 Fg^{-1} at 0.5 Ag^{-1}	90.2 (10,000)	Wang et al. (2024)
R-CoFe LDHs//HC	0.5M $(NH_4)_2SO_4$	238.3 Fg^{-1} at 0.5 Ag^{-1}	90.4 (10,000)	Wang et al. (2023)
rGO/$CdMoO_4$	**6M KOH**	**99 Fg^{-1} at 5 mVs^{-1}**	77, 9 (5,000)	**This work**
rGO/$CdWO_4$		**38 Fg^{-1} at 5 mVs^{-1}**	77, 3 (5,000)	

The bold letters represent materials and response of the present work.

4 Discussion

In this study, we identified a hybrid rGO/NPs multilayer nanoarchitecture that demonstrated significant improvements in specific capacitance compared to rGO alone. This improvement can be attributed to two key factors: first, an increase in the electrode surface area, which occurs when the nanoparticles help to maintain the separation between the rGO layers; and second, an improvement in conductivity facilitated by the bridging effect of the nanoparticles (Das et al., 2024), which connects the top and bottom rGO layers in the out-of-plane direction. The better performance of the composite rGO/$CdMoO_4$ in comparison to rGO/$CdWO_4$ can be understand in terms of the size of the synthesized nanoparticles. As illustrated in SEM images of the Figure 2 and corresponding particle size calculations, it is very clear that the average size of the $CdMoO_4$ nanoparticles are much smaller (~42.5 nm) than the average size of the $CdWO_4$ nanoparticles (~300 nm). The smaller size of the nanoparticle result into higher surface area of the material and hence of the electrode too. Moreover, the smaller size of the particles helps to increase the ionic conductivity due to bridging effect too. The smaller the nanoparticle, the more particles land on the graphene layers, and the more likely the NPs are to align for the bridging effect to occur. Conversely, the larger the NPs are, the less likely they are to align between the interlayers, resulting in a smaller bridging effect. In our case, the $CdMoO_4$ nanoparticles are of much smaller, size, leading to a higher likelihood of conductivity due to the bridging effect and, consequently, a higher specific capacitance compared to $CdWO_4$. Figure 10 shows a schematic diagram of the bridging effect explaining higher specific capacitance and hence better performance of supercapacitor based on rGO/$CdMoO_4$ material.

Finally, a comparative table between capacitance values and retention of different materials that stand out in the literature with those found in this work, can be seen in Table 3. We observe that the discrepancy between these materials and the one of this work is small and is compensated and benefitted over by the fast synthesis process and the low costs involved in using the microwave-assisted method, so it would be interesting to extend studies of microwave synthesis for this type of application.

5 Conclusion

In this work, we have proposed that hybrid architectures of rGO/$CdMoO_4$ and rGO/$CdWO_4$ nanostructures which significantly improve the specific capacitance compared to bare rGO. This enhancement in the performance can be caused by two effects (Liu et al., 2010): the increase in surface area due to the presence of the smaller NPs, which prevents the graphene layers from collapsing into each other, and (Dissanayake and Kularatna-Abeywardana, 2024) a bridging effect that occurs due to the alignment of the NPs which increases the conductivity. The rapid and low-cost synthesis using the microwave-assisted method allowed for obtaining 42.5 nm $CdMoO_4$ nanoparticles and 300 nm $CdWO_4$ nanoparticles. The rGO/$CdMoO_4$-based electrodes exhibited a high specific capacitance, energy density, and power density, with a remarkable 77% retention after 5,000 charge/discharge cycles, highlighting their stability and efficiency. These results suggest that rGO/$CdMoO_4$ composites have great potential for application in energy storage devices, offering an attractive balance between performance and cost.

Data availability statement

The original contributions presented in the study are included in the article/supplementary material, further inquiries can be directed to the corresponding author.

Author contributions

LV: Conceptualization, Data curation, Formal Analysis, Investigation, Methodology, Supervision, Writing–original draft, Writing–review and editing. CM: Data curation, Investigation, Methodology, Visualization, Writing–original draft. DP: Formal Analysis, Investigation, Writing–review and editing. PM: Formal Analysis, Investigation, Writing–review and editing. DS: Conceptualization, Investigation, Writing–review and editing.

Funding

The author(s) declare that financial support was received for the research, authorship, and/or publication of this article. This research was funded by ANID-Millennium Science Initiative Program ICN17_012, ANID-Fondecyt Regular 1231714 Chile.

Conflict of interest

The authors declare that the research was conducted in the absence of any commercial or financial relationships that could be construed as a potential conflict of interest.

Generative AI statement

The author(s) declare that no Generative AI was used in the creation of this manuscript.

Publisher's note

All claims expressed in this article are solely those of the authors and do not necessarily represent those of their affiliated organizations, or those of the publisher, the editors and the reviewers. Any product that may be evaluated in this article, or claim that may be made by its manufacturer, is not guaranteed or endorsed by the publisher.

References

Alam, S. N., Sharma, N., and Kumar, L. (2017). Synthesis of graphene oxide (GO) by modified Hummers method and its thermal reduction to obtain reduced graphene oxide (rGO). *Graphene* 06 (01), 1–18. doi:10.4236/graphene.2017.61001

Anitha, T., Reddy, A. E., Anil Kumar, Y., Cho, Y. R., and Kim, H. J. (2019). One-step synthesis and electrochemical performance of a $PbMoO_4$/$CdMoO_4$ composite as an electrode material for high-performance supercapacitor applications. *Dalton Trans.* 48 (28), 10652–10660. doi:10.1039/c9dt01931f

Bahmani, F., Kazemi, S. H., Wu, Y., Liu, L., Xu, Y., and Lei, Y. (2019). CuMnO2-reduced graphene oxide nanocomposite as a free-standing electrode for high-performance supercapacitors. *Chem. Eng. J.* 375, 121966. doi:10.1016/j.cej.2019.121966

Bermúdez, J. M., Beneroso, D., Rey-Raap, N., Arenillas, A., and Menéndez, J. A. (2015). Energy consumption estimation in the scaling-up of microwave heating processes. *Chem. Eng. Process. Process Intensif.* 95, 1–8. doi:10.1016/j.cep.2015.05.001

Chan, C. H., Ab Manap, N. I., Nek Mat Din, N. S. M., Ahmad Hazmi, A. S., Kow, K. W., and Ho, Y. K. (2021). Strategy to scale up microwave synthesis with insight into the thermal and non-thermal effects from energy-based perspective. *Chem. Eng. Process. - Process Intensif.* 168, 108594. doi:10.1016/j.cep.2021.108594

Chang, J., Mane, R. S., Ham, D., Lee, W., Cho, B. W., Lee, J. K., et al. (2007). Electrochemical capacitive properties of cadmium oxide films. *Electrochim Acta* 53 (2), 695–699. doi:10.1016/j.electacta.2007.07.056

Cuéllar-Herrera, L., Arce-Estrada, E. M., Pacheco-Catalán, D. E., Vivas, L., Ortiz-Landeros, J., Jiménez-Lugos, C., et al. (2024). Chemical synthesis and electrochemical performance of Hausmannite Mn_3O_4/rGO composites for supercapacitor applications. *Int. J. Electrochem Sci.* 19 (9), 100737. doi:10.1016/j.ijoes.2024.100737

Cui, M., and Meng, X. (2020). Overview of transition metal-based composite materials for supercapacitor electrodes. *Nanoscale Adv.* 2 (12), 5516–5528. doi:10.1039/d0na00573h

Das, P., Ibrahim, S., Chakraborty, K., Ghosh, S., and Pal, T. (2024). Stepwise reduction of graphene oxide and studies on defect-controlled physical properties. *Sci. Rep.* 14 (1), 294. doi:10.1038/s41598-023-51040-0

Daturi, M., Busca, G., Borel, M. M., Leclaire, A., and Piaggio, P. (1997). Vibrational and XRD study of the system $CdWO_4$ –$CdMoO_4$. *J. Phys. Chem. B* 101 (22), 4358–4369. doi:10.1021/jp963008x

Dissanayake, K., and Kularatna-Abeywardana, D. (2024). A review of supercapacitors: materials, technology, challenges, and renewable energy applications. *J. Energy Storage* 96, 112563. doi:10.1016/j.est.2024.112563

Dubey, R., and Guruviah, V. (2019). Review of carbon-based electrode materials for supercapacitor energy storage. *Ionics (Kiel)* 25 (4), 1419–1445. doi:10.1007/s11581-019-02874-0

Faraji, S., and Ani, F. N. (2014). Microwave-assisted synthesis of metal oxide/hydroxide composite electrodes for high power supercapacitors – a review. *J. Power Sources* 263, 338–360. doi:10.1016/j.jpowsour.2014.03.144

Ferrari, A. C. (2007). Raman spectroscopy of graphene and graphite: disorder, electron–phonon coupling, doping and nonadiabatic effects. *Solid State Commun.* 143 (1–2), 47–57. doi:10.1016/j.ssc.2007.03.052

Fu, C., Kuang, Y., Huang, Z., Wang, X., Yin, Y., Chen, J., et al. (2011). Supercapacitor based on graphene and ionic liquid electrolyte. *J. Solid State Electrochem.* 15 (11–12), 2581–2585. doi:10.1007/s10008-010-1248-9

Jayaraman, A., Wang, S. Y., and Sharma, S. K. (1995). High-pressure Raman investigation on CdMoO4 and pressure-induced phase transformations. *Phys. Rev. B* 52 (14), 9886–9889. doi:10.1103/physrevb.52.9886

Kadam, S. R., Panmand, R. P., Tekale, S., Khore, S., Terashima, C., Gosavi, S. W., et al. (2018). Hierarchical CdMoO4 nanowire–graphene composite for photocatalytic hydrogen generation under natural sunlight. *RSC Adv.* 8 (25), 13764–13771. doi:10.1039/c8ra01557k

Kalia, S., Choudhary, D., Shrivastav, M., Bala, R., Singh, R. K., Khan, M. S., et al. (2024). Synergistic effects of Ag nanoparticles in the rGO and Co_3O_4 based electrode materials for asymmetric supercapacitors. *Electrochim Acta* 491, 144337. doi:10.1016/j.electacta.2024.144337

Kim, D., Seol, S. K., and Chang, W. S. (2016). Energy efficiency of a scaled-up microwave-assisted transesterification for biodiesel production. *Korean J. Chem. Eng.* 33 (2), 527–531. doi:10.1007/s11814-015-0184-x

Kumar, E. P., Chanakya, N., Siddiqua, A., Krishna, K. G., Kumar, B. V., Muralikrishna, P., et al. (2024). Investigations on MWO4 (M = Cu, Zn, Cd and Sn) nanostructures for detecting toluene gas at room temperature. *Sens. Actuators A Phys.* 368, 115094. doi:10.1016/j.sna.2024.115094

Lehmann, H. (2007). Scale-up in microwave-accelerated organic synthesis. *Ernst Scher. Found. Symp. Proc.*, 133–149. doi:10.1007/2789_2007_032

Li, X. Q., Chang, L., Zhao, S. L., Hao, C. L., Lu, C. G., Zhu, Y. H., et al. (2017). Research on carbon-based electrode materials for supercapacitors. *Acta Physico-Chimica Sin.* 33 (1), 130–148. doi:10.3866/pku.whxb201609012

Lim, C. S. (2012). Microwave-assisted synthesis of $CdWO_4$ by solid-state metathetic reaction. *Mater Chem. Phys.* 131 (3), 714–718. doi:10.1016/j.matchemphys.2011.10.039

Liu, C., Li, F., Ma, L., and Cheng, H. (2010). Advanced materials for energy storage. *Adv. Mater.* 22 (8), E28–E62. doi:10.1002/adma.200903328

Liu, H., and Tan, L. (2010). Synthesis, structure, and electrochemical properties of $CdMoO_4$ nanorods. *Ionics (Kiel)* 16 (1), 57–60. doi:10.1007/s11581-009-0345-1

Long, J. W., Brousse, T., and Bélanger, D. (2015). Electrochemical capacitors: fundamentals to applications. *J. Electrochem Soc.* 162 (5), Y3. doi:10.1149/2.0261505jes

Marcano, D. C., Kosynkin, D. V., Berlin, J. M., Sinitskii, A., Sun, Z., Slesarev, A., et al. (2010). Improved synthesis of graphene oxide. *ACS Nano* 4 (8), 4806–4814. doi:10.1021/nn1006368

Moghadam, M. T. T., Babamoradi, M., and Azimirad, R. (2019). Effect of hydrothermal reaction temperature on the photocatalytic properties of CdWO4-RGO nanocomposites. *J. Nanostructures* 9 (4), 600–609. doi:10.22052/JNS.2019.04.001

Patil, S., Raut, S., Gore, R., and Sankapal, B. (2015). One-dimensional cadmium hydroxide nanowires towards electrochemical supercapacitor. *New J. Chem.* 39 (12), 9124–9131. doi:10.1039/c5nj02022k

Phuruangrat, A., Ekthammathat, N., Thongtem, T., and Thongtem, S. (2011). Microwave-assisted synthesis and optical property of CdMoO4 nanoparticles. *J. Phys. Chem. Solids* 72 (3), 176–180. doi:10.1016/j.jpcs.2010.12.003

Rajagopalan, B., and Chung, J. S. (2014). Reduced chemically modified graphene oxide for supercapacitor electrode. *Nanoscale Res. Lett.* 9 (1), 535. doi:10.1186/1556-276x-9-535

Raut, S. S., and Sankapal, B. R. (2016). First report on synthesis of $ZnFe_2O_4$ thin film using successive ionic layer adsorption and reaction: approach towards solid-state symmetric supercapacitor device. *Electrochim Acta* 198, 203–211. doi:10.1016/j.electacta.2016.03.059

Ren, P. G., Yan, D. X., Ji, X., Chen, T., and Li, Z. M. (2011). Temperature dependence of graphene oxide reduced by hydrazine hydrate. *Nanotechnology* 22 (5), 055705. doi:10.1088/0957-4484/22/5/055705

Ritter, T. G., Pappu, S., and Shahbazian-Yassar, R. (2024). Scalable synthesis methods for high-entropy nanoparticles. *Adv. Energy Sustain. Res.* 5 (8). doi:10.1002/aesr.202300297

Shabani Shayeh, J., Norouzi, P., and Ganjali, M. R. (2015). Studying the supercapacitive behavior of a polyaniline/nano-structural manganese dioxide composite using fast Fourier transform continuous cyclic voltammetry. *RSC Adv.* 5 (26), 20446–20452. doi:10.1039/c4ra16801a

Shejini, R., Mohanraj, K., Soon Min, H., Henry, J., and Sivakumar, G. (2024). Designing the redox activity of $CuMoO_4$ electrodes on N-rich reduced graphene oxide nanocomposite for high performance supercapacitor. *Solid State Sci.* 154, 107586. doi:10.1016/j.solidstatesciences.2024.107586

Shelke, N. T., Yewale, M. A., Kadam, R. A., Kumar, V., Teli, A. M., Beknalkar, S. A., et al. (2024). Synthesis of $Ni_3V_2O_8$-rGO composite nanostructure for high-performance hybrid supercapacitors via hydrothermal method. *Diam. Relat. Mater* 146, 111171. doi:10.1016/j.diamond.2024.111171

Sheoran, K., Thakur, V. K., and Siwal, S. S. (2022). Synthesis and overview of carbon-based materials for high performance energy storage application: a review. *Mater Today Proc.* 56, 9–17. doi:10.1016/j.matpr.2021.11.369

Sofronov, D., Sofronova, E., Starikov, V., Baymer, V., Kudin, K., Matejchenko, P., et al. (2012). Microwave synthesis of tetragonal phase $CdWO_4$. *Mater. Manuf. Process.* 27 (5), 490–493. doi:10.1080/10426914.2011.593229

Sun, Z., Han, X., and Wang, D. (2023). Zinc-iodine battery-capacitor hybrid device with excellent electrochemical performance enabled by a robust iodine host. *J. Energy Storage* 62, 106857. doi:10.1016/j.est.2023.106857

Vimuna, V. M., Karthika, U. M., Alex, S., and Xavier, T. S. (2022). Microsphere rGO/MnO2 composites as electrode materials for high-performance symmetric supercapacitors synthesized by reflux reaction. *Inorg. Chem. Commun.* 141, 109508. doi:10.1016/j.inoche.2022.109508

Vivas, L., Jara, A., Garcia-Garfido, J. M., Serafini, D., and Singh, D. P. (2022). Facile synthesis and optimization of CrOOH/rGO-Based electrode material for a highly efficient supercapacitor device. *ACS Omega* 7 (46), 42446–42455. doi:10.1021/acsomega.2c05670

Vivas, L., and Singh, D. P. (2022). A highly efficient graphene gold based green supercapacitor coin cell device for energy storage. *Front. Energy Res.* 9. doi:10.3389/fenrg.2021.794604

Wang, D., Han, X., and Zhang, X. (2024). Achieving high-capacity aqueous calcium-ion storage in amorphous manganese oxide nanospheres for calcium-ion asymmetric supercapacitors. *J. Power Sources* 599, 234215. doi:10.1016/j.jpowsour.2024.234215

Wang, D., Sun, J., and Chen, L. (2023). Structural reconstruction strategy enables CoFe LDHs for high-capacity NH_4^+ storage and application in high-energy density ammonium-ion hybrid supercapacitors. *ChemSusChem* 16 (12), e202300207. doi:10.1002/cssc.202300207

Wang, R., Wang, Y., Xu, C., Sun, J., and Gao, L. (2013). Facile one-step hydrazine-assisted solvothermal synthesis of nitrogen-doped reduced graphene oxide: reduction effect and mechanisms. *RSC Adv.* 3 (4), 1194–1200. doi:10.1039/c2ra21825a

Wang, Y., Wu, X., Han, Y., and Li, T. (2021). Flexible supercapacitor: overview and outlooks. *J. Energy Storage* 42, 103053. doi:10.1016/j.est.2021.103053

Xu, J., Wu, M., Chen, M., and Wang, Z. (2015). A one-step method for fabrication of $CdMoO_4$-graphene composite photocatalyst and their enhanced photocatalytic properties. *Powder Technol.* 281, 167–172. doi:10.1016/j.powtec.2015.04.079

Zhao, YHSLH (2024). Flower-like NiCo2S4/rGO composites directly grown on Ni Foam as highly efficient electrode for long cycling stability supercapacitor. *Indian J. Chem.* 63 (8). doi:10.56042/ijc.v63i8.8566

Zhu, Y. J., and Chen, F. (2014). Microwave-assisted preparation of inorganic nanostructures in liquid phase. *Chem. Rev.* 114 (12), 6462–6555. doi:10.1021/cr400366s